materials

MDPI

Article

Stress Relaxation Behavior of Additively Manufactured Polylactic Acid (PLA)

Alcide Bertocco *,†, Matteo Bruno †, Enrico Armentani †, Luca Esposito † and Michele Perrella †

Department of Chemical, Materials and Production Engineering, University of Naples Federico II, Piazzale V. Tecchio 80, 80125 Naples, Italy; matteo.bruno@unina.it (M.B.); enrico.armentani@unina.it (E.A.); luca.esposito2@unina.it (L.E.); michele.perrella@unina.it (M.P.)

* Correspondence: alcide.bertocco@unina.it

† These authors contributed equally to this work.

Abstract: In this work, the stress relaxation behavior of 3D printed PLA was experimentally investigated and analytically modeled. First, a quasi-static tensile characterization of additively manufactured samples was conducted by considering the effect of printing parameters like the material infill orientation and the outer wall presence. The effect of two thermal conditioning treatments on the material tensile properties was also investigated. Successively, stress relaxation tests were conducted, on both treated and unconditioned specimens, undergoing three different strains levels. Analytical predictive models of the viscous behavior of additive manufactured material were compared, highlighting and discussing the effects of considered printing parameters.

Keywords: additive manufacturing; stress relaxation; viscoelasticity; analytical fitting; experimental mechanics; polylactic acid (PLA)

check for updates

Citation: Bertocco, A.; Bruno, M.; Armentani, E.; Esposito, L.; Perrella, M. Stress Relaxation Behavior of Additively Manufactured Polylactic Acid (PLA). *Materials* **2022**, *15*, 3509. https://doi.org/10.3390/ma15103509

Academic Editor: Tomasz Sadowski

Received: 12 April 2022
Accepted: 10 May 2022
Published: 13 May 2022

1. Introduction

Additive manufacturing (AM), or 3D printing, is an advanced technology that enables high-accuracy and low-cost production of physical models and structures of complex geometry. In the last few years, AM significantly evolved in a growing market. Additive-manufactured parts are built layer by layer with deposition of material according to 3D digital design [1–4]. AM technology is currently adopted in a wide range of engineering applications such as mechanical, biomedical, construction, aerospace, and food industries as well as in academic research [5–9]. Currently, many different technologies are available in the AM field and can be classified by means of the energy source or the way the material is joined, for instance, by using a binder, laser or heated nozzle. A classification is also possible by group of materials processed, such as plastics, metals or ceramics [10]. The most common materials used in AM are certainly plastics and polymers in general; nevertheless, the strong technological development has allowed also metallic and ceramic materials to become of interest in this field. Table 1 shows the different materials that can be used in relation to the various technological processes described. Among polymers, polylactic acid (PLA), also known as polylactide, is attracting increasing interest from industry and researchers. PLA is a biodegradable thermoplastic polyester derived from totally renewable resources such as sugar beets and corn [11]. In specific conditions [12], the decomposition of PLA into water, carbon dioxide and humus (the black organic material in soil) can be obtained. Furthermore, PLA shows interesting mechanical properties such as high stiffness and high strength if compared to many synthetic polymers [13]. Physical and mechanical properties of PLA are extensively discussed in [14]. Therefore, PLA is proving to be a potential alternative to replace petroleum-derived polymers [12]. It is used in a variety of bio-medical applications as well such as dialysis media, porous scaffolds, bone-fixation devices, interference screws, drug-eluting stents, sutures, and suture anchors [15–17]. It is noteworthy that untreated PLA has mechanical properties heavily dependent on

temperature and, for this reason, its application is preferable in low-temperature solutions, usually up to 60 °C [18]. On the contrary, an annealing thermal treatment (between glass transition and melt temperatures) could enhance the mechanical properties of FDM–PLA parts [19].

Fused deposition modeling (FDM) is the most popular and affordable AM extrusion-based method to manufacture polymer-based structures. Because of its extensive use, a thorough understanding of the influence of the manufacturing process on the mechanical properties of PLA material is crucial. The quality of products fabricated by the FDM process is usually affected from surface roughness, poor precision and low strength [20]. An opportune selection of printing parameters, such as temperature, printing speed, wall thickness and layer height, can significantly improve the overall printed samples quality [21,22]. The mechanical behavior of polymeric structures is mainly governed by time dependent rheological effects, and therefore, the prediction of the inelastic mechanical behavior, in terms of monotonic and cycling loading, as well as creep and relaxation, is of great importance [23,24]. The viscoelastic behavior of polymers strongly influences the optimal choice of their fields of application. The viscoelasticity of materials is exhibited in different ways, such as the progressive deformation of a material sample under constant stress, i.e., creep behavior, and the gradual reduction in force when the sample is subject to a constant strain, i.e., stress relaxation. In general, viscoelasticity is a phenomenon associated with time-dependent material response [25]. Biodegradable polymers can undergo failure much before the anticipated yielding and ultimate tensile strength, due to its viscous nature, which leads to the creep or relaxation rupture. For example, in Grabow et al. [26], significant creep deformation in PLA stents was reported when subjected to a constant load. Up to the proportionality limit, deformation occurring in the polymer specimen is similar to the uncoiling of a molecular chain. No intermolecular slippage is noticed, and strains are recoverable in this area but only after a certain period. The deformation that occurs beyond this proportionality limit is unrecoverable. These distortions occur due to the actual displacement of the molecules over each other, which causes permanent deformation [27,28]. In [29], the creep behavior of biodegradable PLA was analyzed, considering the effects of layer thickness and printing angle. Creep response was also modeled by using Burger model for predictive purposes. The static properties of printed PLA and their dependency on printing parameters have been extensively studied, and many works are available on these topics. On the other hand, although several papers have dealt with the investigation of creep behavior of printed PLA materials, the literature on stress relaxation response of PLA subject to thermal ageing is limited. In this work, an investigation of the viscoelastic behavior of the PLA as a function of the infill strategy is presented. First, the static characterization of PLA samples, printed using different infill orientations, was carried out. Afterwards, an extensive campaign of stress relaxation tests was conducted. Here, the influence of infill strategy was taken into account. Finally, analytical predictive models to describe the relaxation behavior of the PLA printed by FDM technology were described and compared. The presented results can be useful for expanding the use of PLA material in the 3D printing of products for further engineering sectors.

Table 1. Materials for additive manufacturing and related technological processes.

Technology	Polymers	Metals	Ceramics	Composites
Stereolithography	•			•
Digital light processing	•			
Multi-jet modeling	•			•
Fused deposition modeling	•			
Electron beam melting		•		
Selective laser sintering	•	•	•	•
Selective heat sintering	•			
Direct metal laser sintering		•		
Plaster-based 3D printing			•	•
Laminated object manufacture	•	•	•	•
Ultrasonic consolidation		•		
Laser metal deposition		•		•

2. Materials and Methods

2.1. Experimental Methods

The experimental campaign was performed on samples printed with a PLA plus filament, by Zhuhai SUNLU Industrial Co., Zhuhai, China, whose nominal properties are reported in Table 2.

Table 2. Nominal PLA filament properties provided by the supplier.

Filament Diameter [mm]	Tensile Strength [N]	Melt Flow Rate [g/10 min]	Transition Temperature T_g [°C]
1.75 ± 0.02	$108 \div 147$	$9 \div 11$	62.5

A commercial FDM linear Cartesian machine, Artilery Sidewinter X1 (Shenzhen Yuntuchuangzhi Technology Co., Ltd., Shenzhen, China), equipped with a direct extrusion system, was adopted to 3D print the material. It was extruded through a 0.4 mm-diameter nozzle with an extrusion temperature of 210 °C and a deposition velocity of 60 mm/s. Other critical printing parameters such as the bed plate temperature and the layers height were set to 50 °C and 0.1 mm, respectively. The manufacturing process was conducted in a controlled environment. Currently, there is no specific standard reference for additively manufactured polymers testing. Therefore, the experimental campaigns presented in this work were conducted by adopting a custom rectangular cross section sample, Figure 1a, with a length in the traction direction equals to 120 mm, a width of 6 mm and a thickness of 3 mm. The gauge length was set to 25 mm. The specimens were clamped using self-tightening wedge grips mounting specific jaws for polymers, thus avoiding specimen distortions due to overly hard clamping. Tests on specimens realized according to ASTM D638 standard were also performed, but the dog bone geometry seemed not suitable for the FDM samples printed with the selected parameters, due to the great deal of breakages in fillets close to the clamping area. A similar premature failure of ASTM D638 printed specimens was also highlighted in [30].

In a standard FDM process, the thermoplastic filament is melted in a liquefier and extruded through a nozzle onto the build platform according to the predetermined tool paths. Once a layer is completed, the extrusion apparatus is raised (or the build platform is lowered), and then the next layer is deposited on the previous one. The whole process is repeated until the entire part geometry is realized [31]. Generally, the FDM technology is characterized by the presence of contour lines, Figure 1b, enclosing the slice section, representing a key factor respect to the workpiece dimensional quality and geometrical

accuracy [32]. Sets of specimens were printed with and without the outer wall, consisting of a single contour line, to investigate the effect of the contour on the mechanical behavior of additive manufactured material. In addition, to evaluate the influence of the printing orientation on the PLA mechanical response, three different printing infill directions were tested as schematically reported in Figure 1c. The considered infill orientations were $0°, 45°$ and $90°$ respect to the traction direction.Every layer was printed using the same infill direction and automatic stacking strategy was not adopted. Moreover, in order to analyze the mechanical behavior of printed PLA under operative conditions, heat and cold thermal treatments were applied to specimens printed with the $0°$ infill direction, i.e., the configuration providing higher strength. The heating conditioning sequence was obtained by holding the samples for 8 h in an air-circulating oven at a temperature (T_h) of about the 80% of the material transition temperature T_g. The cooling treatment consisted of maintaining the specimens for 8 h in a laboratory freezer at constant $T_c = -15$ °C temperature. The temperature levels selected for the thermal treatments were chosen as representative of operating conditions to simulate the natural aging of the material. In both cases, the specimens returned to room temperature in calm conditions.

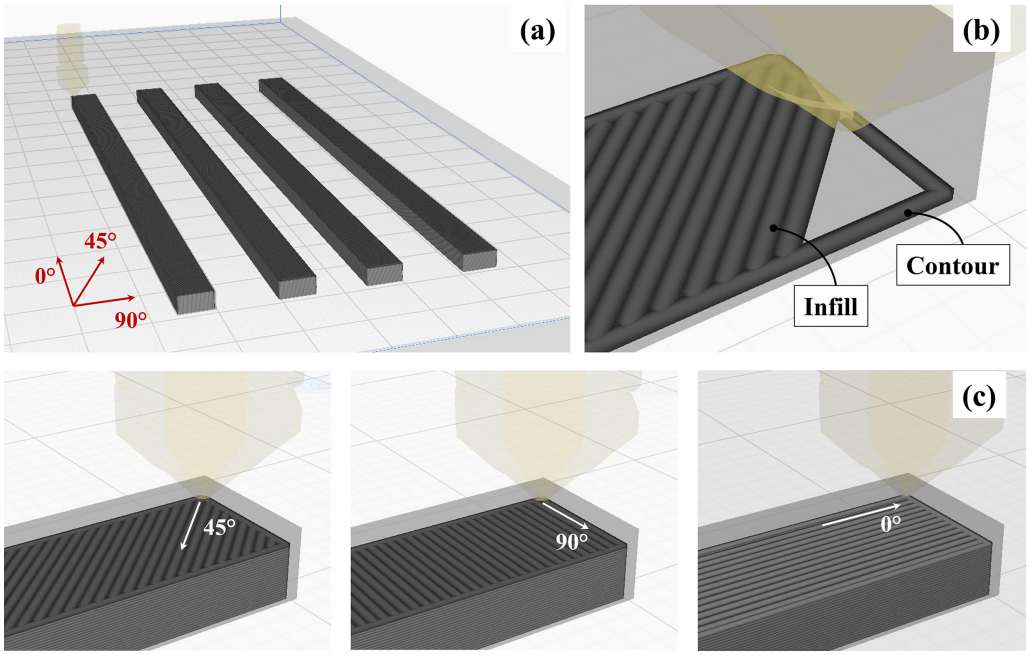

Figure 1. Schematic representation of specimens geometry (**a**), contour and infill lines (**b**) and considered printing direction (**c**).

Quasi-static tensile characterization was conducted to estimate the material elastic properties depending on the infill orientation, the contour influence and thermal conditioning. A servo-hydraulic testing machine Instron 8500 plus (Instron, Buckinghamshire, UK), with a 1 kN load cell, was adopted to execute tensile tests under displacement control. The average elastic modulus and the deformation correspondent to the maximum reached stress were estimated. Successively, experimental stress relaxation characterization of the additively manufactured PLA was executed under strain control. Constant tensile deformation ϵ_o was applied to the specimens and the corresponding engineering stress trend $\sigma(t)$ was evaluated over an assigned dwell time Δt. In the present work, three straining values, respectively, equal to the 27%, 36% and 45% of the deformation at the maximum stress, were considered for the contoured $0°$, $45°$ and $90°$ infill printed direction samples. The relaxation phenomenon was measured over a time $\Delta t = 500$ s.

2.2. Analytical Methods

Three different predictive laws were adopted to model the viscoelastic behavior of PLA samples. A comparison of analytical modeling and an evaluation of the infill direction influence on the relaxation behavior was performed. All the experimental data from the three test strain levels for each infill printing direction were collected in a unique set to identify model parameters. The best data fitting was reported by means of the correlation coefficient. First, a rheological Maxwell model was implemented [33]. As reported in (1), the trend of the stress over the time depends on the imposed straining ϵ_0 level and on the two parameters A_1 and A_2 which, respectively, represent the spring stiffness and the dashpot damping value.

$$\sigma(t) = \epsilon_0 \cdot A_1 \cdot \epsilon^{-t/A_2} \tag{1}$$

Second, a more complex standard Linear Solid model [34] was implemented. In (2), the correspondent formulation for the stress evolution over the time, is reported.

$$\sigma(t) = \epsilon_0 \cdot [B_1 + B_2 \cdot \epsilon^{-t/B_3}] \tag{2}$$

Similar to the Maxwell approach, in the standard linear solid model, the stress is linearly dependent on the imposed strain level ϵ_0 through three elements: a spring with stiffness B_2 and a dashpot with damping coefficient B_3 combined in parallel to a further spring of stiffness B_1. The representations of the above-mentioned Maxwell and Linear Solid rheological models are reported in Figure 2a,b, respectively.

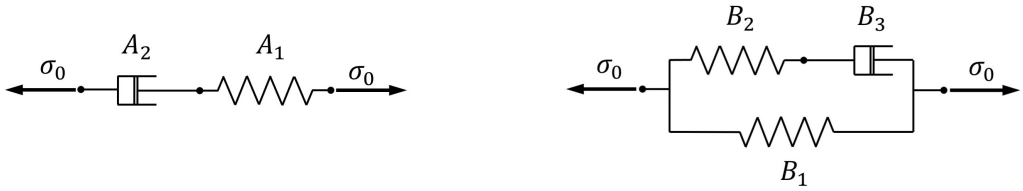

(**a**) (**b**)

Figure 2. Scheme of the considered linear rheological models: (**a**) Maxwell model and (**b**) Linear Solid model.

Finally, the nonlinear *Findley* model was enforced [35]. According to (3), the evolution of stress over time results to be function of the initial stress value σ_0 at the time $t = 0$, the stress-dependent fitting parameter σ_1, the fitting exponent n and of the material constant t_c that was considered as unitary in the present study, according to literature [36,37].

$$\sigma(t) = \sigma_0 + \sigma_1 \cdot (t/t_c)^n \tag{3}$$

Since the purpose of this work is the estimation of relaxation influence on the elastic properties, the presented analytical models were analyzed in terms of creep modulus $E(t)$, obtained by dividing the stress over time $\sigma(t)$ by the constant deformation value ϵ_0, as reported in (4).

$$E(t) = \frac{\sigma(t)}{\epsilon_0} \tag{4}$$

In the following Table 3, the resultant creep modulus expression and the fitting constants are reported for each considered model. It is worth noting that only the parameters σ_0 and σ_1 of Findley law modified their nomenclature in E_0 and C due to the division by remote strain.

Table 3. Considered analytical models creep modulus expression and fitting constants.

	Maxwell	**Linear Solid**	**Findley**
Creep Modulus	$A_1 \cdot e^{-t/A_2}$	$B_1 + B_2 \cdot e^{-t/B_3}$	$E_0 + C \cdot t^n$
Material Constants	$A_1; A_2$	$B_1; B_2; B_3$	$C; n$

Experimental curve fitting was achieved, implementing the creep modulus expression on the MatLab Curve Fitting Toolbox, adopting the non-linear least squares method with the trust region fit option enabled. The R-squared (R^2) values were compared to determine the most accurate model for the experimental data fitting. The identified law was adopted to appreciate the influence of the material infill direction, as well as the thermal conditioning, on the relaxation behavior of the tested 3D printed PLA.

3. Results and Discussion

3.1. Experimental Quasi-Static and Long-Term Behavior

With the purpose to estimate the elastic behavior of the AM material, three tensile tests were performed on each specimen type. The elastic modulus E, the tensile strength σ^* and the correspondent deformation ϵ^* of the contoured specimen type were reported in Table 4 collected by the material infill direction.

Table 4. Elastic characterization of contoured specimens.

Infll Direction	**0°**	**45°**	**90°**
E [MPa]	3045 ± 3	2914 ± 3	2932 ± 3
σ^* [MPa]	60 ± 3	54 ± 3	47 ± 3
ϵ^*	2.75%	2.05%	1.75%

The 0° specimens resulted in the higher values of the elastic modulus, strength and correspondent deformation at peak stress. The 45° samples presented a drop in the elastic modulus of about 5% and a reduction in strength of 10%, while the 90° specimens carried out a tensile strength lower than 21% with respect to the 0° direction. The effect of contour was estimated and representative results for the 45° and for 90° infill direction are, respectively, reported in Figure 3a,b. A comparison with the correspondent contoured specimen outcomes is also shown in the same figure. The different behavior could be related to the way the infill lines are loaded. Indeed, in the 0° specimens all the filament lines were aligned to the loading direction. Therefore, they were loaded along their axis. Instead, the 90° specimens were orthogonal to the load, thus the resultant interface between adjacent filaments was much more stressed than in the 0° specimens. Moreover, samples with an outer wall presented contour lines always oriented at 0°, i.e., the stiffer direction. Despite only one outer wall line being used, the experimental stress–strain curves of contoured 45° and 90° samples were considerably influenced by its presence. The hygroscopic nature of the PLA material [38] and manufacturing flaws can influence the behavior of printed samples. Within this context, thermal treatments, in particular cooling conditioning, could provide performance degradation.

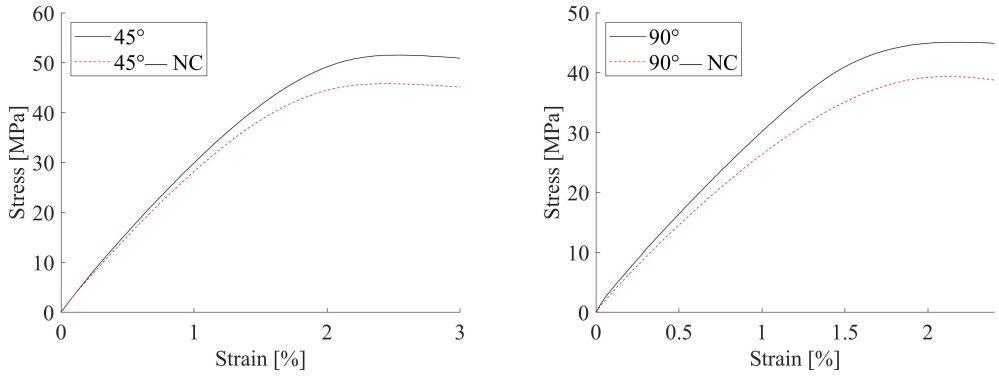

(**a**) (**b**)

Figure 3. Contoured vs. not contoured specimens tensile curves; (**a**) 45° infill orientation; (**b**) 90° infill orientation.

A reduction in strength was noticeable and not influenced by the infill direction, with a drop of about 16% for both the considered directions, while negligible variations were appreciated in the elastic modulus. Furthermore, the influence of thermal treatments on the material elastic properties were estimated through tensile tests conducted on 0° conditioned specimens; the results are reported in Table 5.

Table 5. Elastic characterization of thermally conditioned 0° specimens.

Conditioning	T_h **= 50 °C**	T_c **= −15 °C**
E [MPa]	3005 ± 3	2990 ± 3
σ^* [MPa]	46 ± 3	43 ± 3
ϵ^*	1.56%	1.65%

The quasi-static tensile behavior of thermal conditioned sets is graphically reported in Figure 4. In comparison with the untreated material, a fairly negligible difference (<3%) was detectable in elastic modulus, whilst a decay of about 25–29% in strength was noticed. The cooled specimens were demonstrated to have worse mechanical behavior.

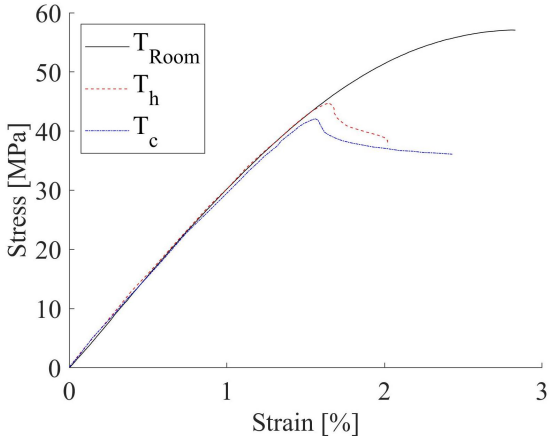

Figure 4. Tensile curves of 0° specimens thermally treated and unconditioned.

The stress relaxation behavior of printed PLA material was investigated and the results discussed in term of normalized creep modulus over time. The normalized creep modulus was computed as the ratio between the creep modulus (4) and the average elastic modulus above was presented. The relaxation results, for the imposed strain values, were reported collected by the infill printing orientation, in Figure 5a for the 0°, in Figure 5b for 45° and in Figure 5c for 90° infill orientation.

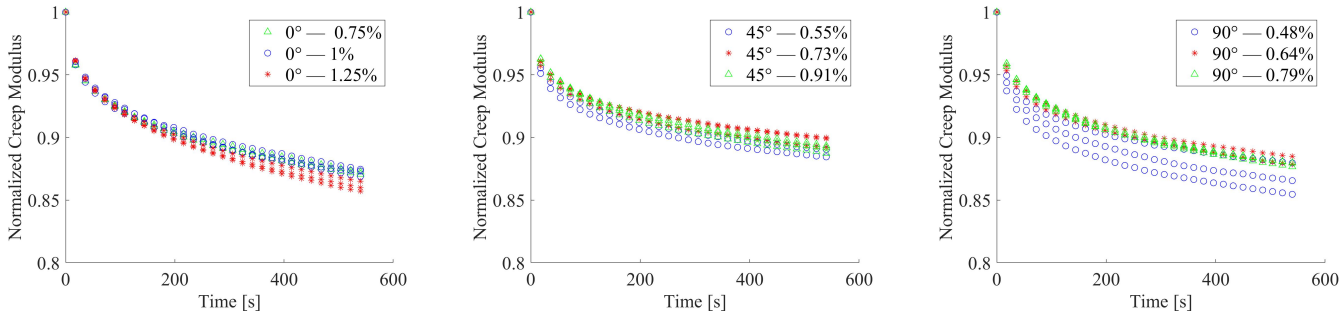

(**a**) (**b**) (**c**)

Figure 5. Normalized creep modulus over time at room temperature; (**a**) 0° infill orientation; (**b**) 45° infill orientation; (**c**) 90° infill orientation.

It is worth noting that samples printed with 90° orientation seem to exhibit non-linear viscoelastic behavior. This response could be ascribed to the way the material is loaded with respect to the infill lines orientation. The 90° samples lay orthogonally to the loading direction, and the sample's response was much more influenced by the interface behavior of adjacent infill lines and eventual flaws.

The 0° and 45° tested specimens resulted in less dispersed data compared to that showed by the 90° specimens. The average creep modulus decay, in the investigated Δt, was estimated to be equal to about 13%, 11% and 13%, respectively, for 0° and 45° and 90°. The outcomes of relaxation tests on the thermally conditioned 0° specimens, here reported in Figure 6a with regard to heating treatment and in Figure 6b for those subject to cooling, showed higher data scatter than unconditioned ones. Both thermal treatments produced an increment of the creep modulus decay with respect to the unconditioned test outcomes.

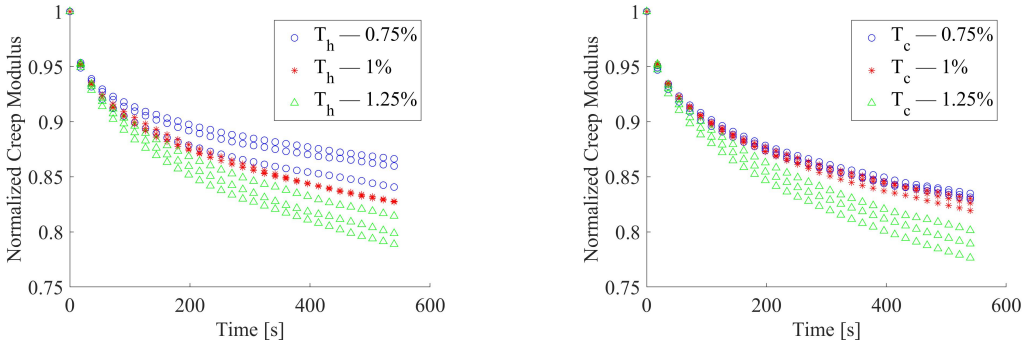

(**a**) (**b**)

Figure 6. Normalized creep modulus over time for thermally conditioned 0° specimens; (**a**) Thermal conditioning T = 50 °C; (**b**) Thermal conditioning T = −15 °C.

3.2. Analytical Modeling of Stress Relaxation Response

The above-proposed analytical models were implemented to fit experimental data sets with all the adopted strain levels. In such a way, the effect of the infill direction on the material relaxation behavior was highlighted. To estimate the models' fitting quality, the coefficient of determination (R-squared) values were computed and reported in Table 6. With respect to the Maxwell and Linear Solid relationships, the Findley model resulted in the higher average value of R^2, always over 0.85.

Table 6. Analytical models R-squared values for the 0°, 45° and 90° infill orientation.

R^2	0°	45°	90°
Maxwell	0.87	0.80	0.73
Linear Solid	0.96	0.92	0.84
Findley	0.97	0.94	0.85

A graphical representation of the Findley empirical model outputs and the experimental outcomes, in terms of normalized creep modulus, is presented in Figure 7a for 0°, in Figure 7b for 45°, and in Figure 7c for the 90° infill direction.

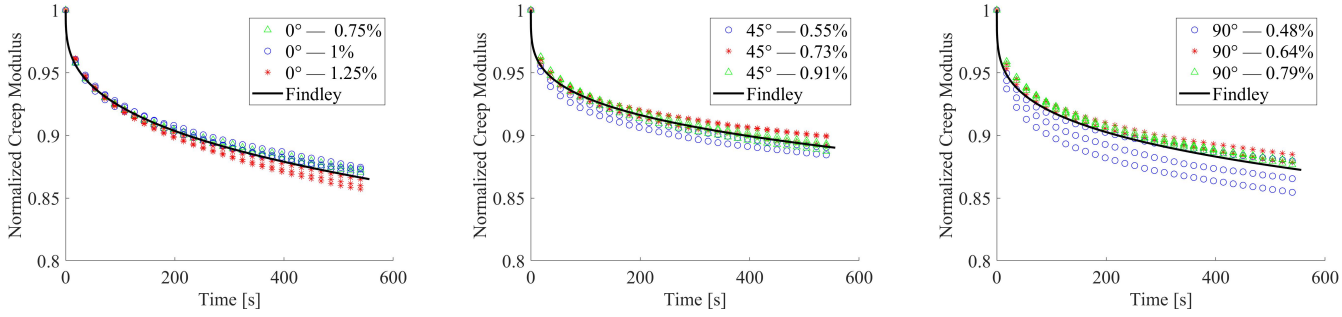

(**a**) (**b**) (**c**)

Figure 7. Trend of normalized creep modulus at room temperature; (**a**) 0° infill orientation; (**b**) 45° infill orientation; (**c**) 90° infill orientation.

The same analytical fitting procedure was applied to the experimental relaxation results of thermally conditioned specimens. The R^2 values, carried out by the analyses of analytical models, are listed in Table 7. Furthermore, for the treated specimens, the Findley law showed a satisfactory prediction of response, with R^2 values always over 0.93.

Table 7. R-squared values from data fitting of the thermally conditioned specimens.

R^2	T_h	T_c
Maxwell	0.87	0.80
Linear Solid	0.96	0.92
Findley	0.97	0.94

Among the investigated predictive models, the Findley equation resulted in the best experimental data fitting, independent of the infill orientation and thermal treatment. Thus, it was selected for comparing the stress relaxation behavior of the untreated and thermally conditioned specimens with different infill orientations. The computed values of Findley model parameters are presented in Table 8 for all the considered testing conditions and manufacturing processes.

Table 8. Findley model parameters for the treated and unconditioned specimens.

	Specimen Type	C	*n*
Untreated	0°	−51.4605	0.3283
	45°	−60.0284	0.2650
	90°	−70.6612	0.2636
Treated	T_h	−59.1985	0.3462
	T_c	−57.7070	0.3604

The comparison among the analytical curves for all the investigated cases is reported in Figure 8. It shows that the material relaxation behavior is hardly influenced by the infill printing direction. Indeed, the normalized creep modulus decreased in the range of 11–14%. From a practical point of view, a difference of about 3% can be considered negligible. The thermal conditioning procedures affected relaxation response of printed PLA, showing a stress decay greater than 45% with respect to the untreated samples.

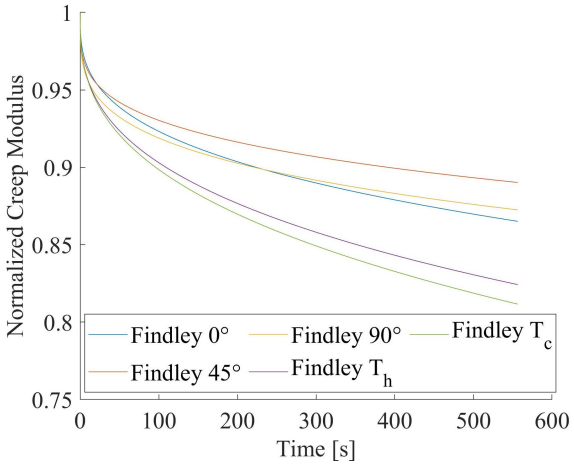

Figure 8. Comparison of stress relaxation curves by Findley model.

4. Conclusions

In this study, three different printing infill directions (0°, 45° and 90°) were considered for evaluating the tensile behavior of printed PLA by FDM technique. The presence of a single-line outer wall was also analyzed. The tensile strength of contoured 0° and 45° specimens was higher than about 17% of the ones without an outer wall. From an operational point of view, the presence of the contour increases the dimensional accuracy of the product.

Secondly, the stress relaxation response was experimentally investigated under different uniaxial strain levels at room temperature. Stress decay ranging from 11% to 14% was acquired. Three analytical models were used for describing stress relaxation response: Maxwell equation, standard Linear Solid model and Findley law. Among them, the Findley empirical expression was confirmed as being the most suitable predicting the tested PLA.

Furthermore, two thermal conditioning procedures were considered for 0° samples in order to reproduce the natural ageing of materials. Both cooled and heated specimens provided a degradation of quasi-static and long-term material properties.

The presented outcomes pointed out the significance of stress relaxation effects in AM PLA structures. Thus, a preliminary predictive analysis should be considered to guarantee reliability over time of 3D printed parts in applications with imposed displacements, e.g., medical brace prostheses or screw joints.

Author Contributions: Conceptualization, A.B., M.B. and M.P.; methodology, E.A., L.E. and M.P.; validation, E.A., L.E. and M.P.; formal analysis, A.B., M.B. and M.P.; writing—original draft preparation, A.B. and M.B.; writing—review and editing, E.A., L.E. and M.P.; supervision, E.A., L.E. and M.P.; All authors have read and agreed to the published version of the manuscript.

Funding: This research received no external funding.

Institutional Review Board Statement: Not applicable.

Informed Consent Statement: Not applicable.

Data Availability Statement: The data that support the findings of this study are available from the corresponding author upon reasonable request.

Conflicts of Interest: All the authors declare that they have no known competing financial interest or personal relationships that could have appeared to influence the work reported in this paper.

Abbreviations

The following abbreviations are used in this manuscript:

PLA	Polylactic Acid
AM	Additive Manufacturing
FDM	Fused Deposition Modeling

References

1. Gebhardt, A. *Understanding Additive Manufacturing*; Elsevier: Amsterdam, The Netherlands, 2011; pp. I–IX. [CrossRef]
2. Shanmugam, V.; Das, O.; Babu, K.; Marimuthu, U.; Veerasimman, A.; Johnson, D.J.; Neisiany, R.E.; Hedenqvist, M.S.; Ramakrishna, S.; Berto, F. Fatigue behaviour of FDM-3D printed polymers, polymeric composites and architected cellular materials. *Int. J. Fatigue* **2021**, *143*, 106007. [CrossRef]
3. Bertocco, A.; Iannitti, G.; Caraviello, A.; Esposito, L. Lattice structures in stainless steel 17-4PH manufactured via selective laser melting (SLM) process: Dimensional accuracy, satellites formation, compressive response and printing parameters optimization. *Int. J. Adv. Manuf. Technol.* **2022**, *120*, 4935–4949. [CrossRef]
4. Citarella, R.; Giannella, V. Additive Manufacturing in Industry. *Appl. Sci.* **2021**, *11*, 840. [CrossRef]
5. Dilberoglu, U.M.; Gharehpapagh, B.; Yaman, U.; Dolen, M. The Role of Additive Manufacturing in the Era of Industry 4.0. *Procedia Manuf.* **2017**, *11*, 545–554. [CrossRef]
6. Harun, W.S.; Manam, N.S.; Kamariah, M.S.; Sharif, S.; Zulkifly, A.H.; Ahmad, I.; Miura, H. A review of powdered additive manufacturing techniques for Ti-6al-4v biomedical applications. *Powder Technol.* **2018**, *331*, 74–97. [CrossRef]
7. Delgado Camacho, D.; Clayton, P.; O'Brien, W.J.; Seepersad, C.; Juenger, M.; Ferron, R.; Salamone, S. Applications of additive manufacturing in the construction industry—A forward-looking review. *Autom. Constr.* **2018**, *89*, 110–119. [CrossRef]
8. Lipton, J.I.; Cutler, M.; Nigl, F.; Cohen, D.; Lipson, H. Additive manufacturing for the food industry. *Trends Food Sci. Technol.* **2015**, *43*, 114–123. [CrossRef]
9. Gibson, I.; Stucker, D.; Rosen, B. *Additive Manufacturing Technologies*; Springer: Berlin/Heidelberg, Germany, 2015; Volume 17, pp. 245–268.
10. Bertocco, A.; Esposito, L.; Aurino, A.; Borrelli, D.; Caraviello, A. Influence of SLM parameters on the compressive behaviour of lattice structures in 17-4PH stainless steel. In Proceedings of the IOP Conference Series Materials Science and Engineering, High Tatras, Slovakia, 13–15 October 2021; Volume 1.
11. Mirkhalaf, S.M.; Fagerström, M. The mechanical behavior of polylactic acid (PLA) films: Fabrication, experiments and modelling. *Mech. Time-Depend. Mater.* **2021**, *25*, 119–131. [CrossRef]
12. Drumright, R.E.; Gruber, P.R.; Henton, D.E. Polylactic Acid Technology. *Adv. Mater.* **2000**, *12*, 1841–1846. [CrossRef]
13. Averett, R.D.; Realff, M.L.; Jacob, K.; Cakmak, M.; Yalcin, B. The mechanical behavior of poly(lactic acid) unreinforced and nanocomposite films subjected to monotonic and fatigue loading conditions. *J. Compos. Mater.* **2011**, *45*, 2717–2726. [CrossRef]
14. Farah, S.; Anderson, D.G.; Langer, R. Physical and mechanical properties of PLA, and their functions in widespread applications—A comprehensive review. *Adv. Drug Deliv. Rev.* **2016**, *107*, 367–392. [CrossRef]
15. Takayama, T.; Todo, M.; Tsuji, H. Effect of annealing on the mechanical properties of PLA/PCL and PLA/PCL/LTI polymer blends. *Mech. Behav. Biomed. Mater.* **2011**, *107*, 255–260. [CrossRef]
16. Zhang, X.; Schneider, K.; Liu, G.; Chen, J.; Brüning, K.; Wang, D.; Stamm, M. Structure variation of tensile-deformed amorphous poly(l-lactic acid): Effects of deformation rate and strain. *Polymer* **2011**, *52*, 4141–4149. [CrossRef]
17. Takahashi, K.; Sawai, D.; Yokoyama, T.; Kanamoto, T.; Hyon, S.H. Crystal transformation from the α- to the β-form upon tensile drawing of poly(l-lactic acid). *Polymer* **2004**, *45*, 4969–4976. [CrossRef]
18. Grasso, M.; Azzouz, L.; Ruiz-Hincapie, P.; Zarrelli, M.; Ren, G. Effect of temperature on the mechanical properties of 3D-printed PLA tensile specimens. *Rapid Prototyp. J.* **2018**, *24*, 1337–1346. [CrossRef]
19. Wach, R.A.; Wolszczak, P.; Adamus-Wlodarczyk, A. Enhancement of mechanical properties of FDM-PLA parts via thermal annealing. *Macromol. Mater. Eng.* **2018**, *303*, 1800169. [CrossRef]
20. Dey, A.; Yodo, N. A Systematic Survey of FDM Process Parameter Optimization and Their Influence on Part Characteristics. *J. Manuf. Mater. Process.* **2019**, *3*, 64. [CrossRef]
21. Pérez, M.; Medina-Sánchez, G.; García-Collado, A.; Gupta, M.; Carou, D. Surface Quality Enhancement of Fused Deposition Modeling (FDM) Printed Samples Based on the Selection of Critical Printing Parameters. *Materials* **2018**, *11*, 1382. [CrossRef]
22. Galantucci, L.; Bodi, I.; Kacani, J.; Lavecchia, F. Analysis of Dimensional Performance for a 3D Open-source Printer Based on Fused Deposition Modeling Technique. *Procedia CIRP* **2015**, *28*, 82–87. [CrossRef]
23. Zacharatos, A.; Kontou, E. Nonlinear viscoelastic modeling of soft polymers. *J. Appl. Polym. Sci.* **2015**, *132*, 42141. [CrossRef]
24. Bruno, M.; Carrino, L.; Esposito, L.; Lopresto, V.; Papa, I.; Russo, P.; Viscusi, A. A Numerical Investigation about Temperature Influence on Thermoplastic Hot-Formed Reinforced Composites Under Low-Velocity Impact. In Proceedings of the ESAFORM 2021, 24th International Conference on Material Forming, Liege, Belgium, 14–16 April 2021. [CrossRef]

25. Stankiewicz, A. Fractional Maxwell model of viscoelastic biological materials. *BIO Web Conf.* **2018**, *10*, 02032. [CrossRef]
26. Grabow, N.; Bünger, C.M.; Schultze, C.; Schmohl, K.; Martin, D.P.; Williams, S.F.; Sternberg, K.; Schmitz, K.P. A biodegradable slotted tube stent based on poly(L-lactide) and poly(4-hydroxybutyrate) for rapid balloon-expansion. *Ann. Biomed. Eng.* **2007**, *35*, 2031–2038. [CrossRef]
27. Plaseied, A.; Fatemi, A. Deformation response and constitutive modeling of vinyl ester polymer including strain rate and temperature effects. *J. Mater. Sci.* **2008**, *43*, 1191–1199. [CrossRef]
28. Guedes, R.M.; Singh, A.; Pinto, V. Viscoelastic modelling of creep and stress relaxation behaviour in PLA-PCL fibres. *Fibers Polym.* **2017**, *18*, 2443–2453. [CrossRef]
29. Ye, J.; Yao, T.; Deng, Z.; Zhang, K.; Dai, S.; Liu, X. A modified creep model of polylactic acid (PLA-max) materials with different printing angles processed by fused filament fabrication. *J. Appl. Polym. Sci.* **2021**, *138*, 50270. [CrossRef]
30. Forster, A. *Materials Testing Standards for Additive Manufacturing of Polymer Materials: State of the Art and Standards Applicability*; United States Department of Commerce: Washington, DC, USA, 2015. [CrossRef]
31. Gao, X.; Yu, N.; Li, J. Influence of printing parameters and filament quality on structure and properties of polymer composite components used in the fields of automotive. In *Structure and Properties of Additive Manufactured Polymer Components*; Woodhead Publishing: Shaston, UK, 2020; pp. 303–330. [CrossRef]
32. Blanco, D.; Fernandez, P.; Noriega, A.; Alvarez, B.J.; Valiño, G. Layer Contour Verification in Additive Manufacturing by Means of Commercial Flatbed Scanners. *Sensors* **2020**, *20*, 1. [CrossRef]
33. Schiessel, H.; Metzler, R.; Blumen, A.; Nonnenmacher, T.F. Generalized viscoelastic models: Their fractional equations with solutions. *J. Phys. Math. Gen.* **1995**, *28*, 6567–6584. [CrossRef]
34. Solis-Ortega, R.D.; Dehghani-Sanij, A.A.; Martinez-Hernandez, U. The Assessment of Viscoelastic Models for Nonlinear Soft Materials. In Proceedings of the 2018 7th IEEE International Conference on Biomedical Robotics and Biomechatronics (Biorob), Enschede, The Netherlands, 26–29 August 2018; pp. 1274–1279. [CrossRef]
35. Findley, W.N.; Lai, J.S.; Onaran, K. *Creep and Relaxation of Nonlinear Viscoelastic Materials: With an Introduction to Linear Viscoelasticity*; Dover Publications, Inc.: New York, NY, USA, 1976.
36. Plevris, N.; Triantafillou, T.C. Creep Behavior of FRP-Reinforced Wood Members. *J. Struct. Eng.* **1995**, *121*, 174–186. [CrossRef]
37. Wu, C.; Lin, P.; Murakami, R. Long-term creep behavior of self-reinforced PET composites. *Express Polym. Lett.* **2017**, *11*, 820–831. [CrossRef]
38. Cuiffo, M.A.; Snyder, J.; Elliott, A.M.; Romero, N.; Kannan, S.; Halada, G.P. Impact of the fused deposition (FDM) printing process on polylactic acid (PLA) chemistry and structure. *Appl. Sci.* **2017**, *7*, 579. [CrossRef]